Peer reviewed version

University of Bristol - Explore Bristol Research
General rights

Optimal Inerter-based Shock-strut Configurations

for Landing Gear Touch-down Performance

Yuan Li*, Jason Zheng Jiang†, Simon A. Neild‡
University of Bristol, Bristol, BS8 1TR, United Kingdom

Huailei Wang §
Nanjing University of Aeronautics and Astronautics, Nanjing, 210016, China

This paper investigates the possibility of improving aircraft landing gear touch-down performance by adding an inerter alongside a linear passive shock strut. The inerter is a novel mechanical element with the property that the applied force is proportional to the relative acceleration between its terminals. A simplified landing gear model is presented and the baseline performance of a conventional oleo-pneumatic shock absorber is established. Candidate layouts with linear mechanical components including inerters are considered using three objective functions: the strut efficiency, the maximum strut load and the maximum stroke. It is demonstrated that improved touch-down performance can be achieved with a linear inerter-based configuration. However it is also observed that the potential energy stored in the gear at the end of the first compression stroke exceeds that of the baseline nonlinear system. This suggests a poorer elongation stage might be observed. To address this, an additional constraint on energy dissipation is then considered. To achieve a reduced potential energy, a double-stage compression spring is introduced. With this, inerter-based configurations that provide improvements for the performance indices of interest are identified and presented.

---

* Ph.D. Student, Department of Mechanical Engineering, yl14470@birstol.ac.uk.
† Lecturer of Dynamics and Control, Department of Mechanical Engineering, z.jiang@birstol.ac.uk (corresponding author).
‡ Professor of Dynamics and Control, Department of Mechanical Engineering, simon.neild@birstol.ac.uk.
§ Associate Professor, College of Aerospace Engineering, whlay@nuaa.edu.cn.

I.   Introduction

The shock absorber unit is often regarded as the critical component in the aircraft landing gear [1]. This unit, together with other parts of landing gear such as the tires, is designed to absorb landing impacts and any immoderate shocks transmitted to the fuselage as the aircraft taxis over uneven surfaces [2]. Among all the design operation conditions, the landing touch-down case determines the greatest energy dissipation requirement for the shock absorber and governs its general performance accordingly [3]. Specifically, the design requirement is to dissipate all the impact energy without causing the aircraft to rebound, while considering the greatest energy absorption efficiency and the minimum gear load which represents passenger/crew comfort [4].

At present, most aircraft uses a passive oleo-pneumatic shock absorber due to its high strut efficiency compared to other shock absorbers, alongside considerable energy dissipation ability and good rebound control [5]. Apart from passive devices, active and semi-active control methods have also been proposed as aircraft shock absorbers. Theoretical analysis and experimental validations have been carried out to investigate the advantages of the actively controlled landing gears, such as in [6, 7]. Moreover, different control strategies have been considered for semi-active shock struts, [1, 8, 9] are examples of such studies. Despite the potential benefits of actively or semi-actively controlled shock struts, potential issues remain regarding reliability and maintenance cost.

In the field of vibration suppression, the "inerter" is a relatively new element [10]. Its properties are that the applied force is proportional to the relative acceleration between its two terminals. The introduction of inerter completes the analogy between mechanical and electrical systems, and fundamentally enlarged the range of passive controllers that can be realized by mechanical networks. Performance advantages have been identified for various systems, including vehicle suspensions [11–13], motorcycle steering systems [14, 15], building suspensions [16–18] and railway vehicles [19–21]. The inerter has been successfully deployed in Formula One racing since 2005 [22]. The effects of an inerter on landing gear shimmy behavior have been investigated recently in [23–25]. In this paper ideal inerters are considered, however a real inerter can have a limited bandwidth and may exhibit nonlinearities. The effects of these factors on vibration suppression systems have been reported in [26–28].

In this paper we focus on improving aircraft touch-down performance using a passive shock strut consisting of linear spring, damper and inerter elements. Baseline performances were identified by considering a landing gear with a conventional oleo-pneumatic shock absorber. This paper is organized as follows. In Section II, a simplified landing gear touch-down model is reviewed, together with a brief introduction of a conventional oleo-pneumatic shock absorber. Several landing touch-down performance criteria are then proposed. In Section III, the optimization procedure and candidate shock-strut layouts are introduced. Beneficial inerter-based shock-strut configurations are identified for each performance index. In Section IV, a constraint on the energy dissipation is implemented in the optimization process to maximize the strut efficiency and minimize the maximum strut load. The possibility of using a double-stage supporting spring is then investigated, with beneficial configurations identified. Conclusions are drawn in Section V.

II. Landing gear touch-down model and performance criteria

In this section, a landing gear model and the dynamics of a conventional oleo-pneumatic shock absorber are summarized. In the modelling process, the assumptions regarding some factors were made for the purpose of simplification: the effects of wheel spin-up drag loads and flexibility of the aircraft structure were ignored; a constant damping orifice discharge coefficient and air-compression exponent were assumed in the nonlinear shock absorber model. Further, detailed analyses of such factors are available in the existing literature [29–32]. The model validity was demonstrated via the comparison between the calculated results and drop-test data [33]. Four performance criteria are then proposed according to the design requirements.

A. Landing gear model

To model the touch-down behavior of the landing gear and aircraft, a two-degree-of-freedom (2DoF) model shown in Fig. 1(a) (a modified version of Fig. 1(a) in [33]) is used. Note that this model is designed to capture the first compressive stroke of the shock strut, i.e., from initial contact with the ground to the first point at which the relative velocity of the shock strut is slowed to zero. We define this point as the end of the touch-down process. Angle ϕ represents the rake angle of the strut. The mass of the gear is split into that above the strut and that below it. M_1 denotes

3

the total of the upper gear mass and the fuselage mass acting on the gear and M_2 represents the lower gear mass. The vertical deflections of the two masses are represented by the two DoFs z_1 and z_2, respectively. These deflections are zero just prior to contact being made with the runway. The strut stroke s_s measures the deflection of the shock strut and is expressed by
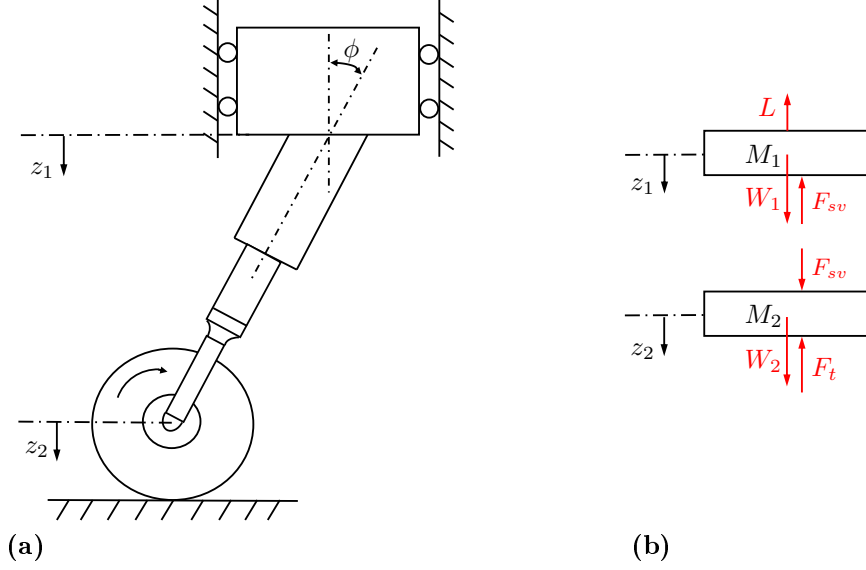
$$s_s = \frac{z_1 - z_2}{\cos \phi}. \tag{1}$$

Fig. 1 View of (a) the dynamic system, (b) free-body diagram of the model.

Fig. 1(b) gives the free-body diagram of the touch-down model. The weight of masses M_1 and M_2 is denoted as W_1 and W_2. The aerodynamic lifting force L and the tire force F_t are applied to the two masses respectively. Specifically, the total aircraft weight is assumed to be fully balanced by lifting force during the full touch-down process, i.e.

$$L = W_1 + W_2. \tag{2}$$

The constant lifting force assumption is based on the fact that the compression stroke is sufficiently quick that the aircraft speed and lift may be considered constant over its duration. This assumption is also used in [5]. Linear force-deflection characteristic of the tire is given by

$$F_t = k_t z_2, \tag{3}$$

4

where k_t is the linear tire stiffness in vertical direction. The vertical force generated by the shock strut is represented by F_{sv}, which is

$$F_{sv} = F_s cos\phi, \tag{4}$$

where F_s is the strut force along the strut axis. The exact expression of F_s will be discussed in Section II.B. Balancing the forces acting on the two masses, the equations of motion for this system are written as follows:

$$\frac{W_1}{g}\ddot{z}_1 + F_{sv} + L - W_1 = 0, \tag{5}$$

$$\frac{W_2}{g}\ddot{z}_2 - F_{sv} + F_t - W_2 = 0, \tag{6}$$

where g denotes the gravitational constant. Eliminating F_{sv} gives

$$\frac{W_1}{g}\ddot{z}_1 + \frac{W_2}{g}\ddot{z}_2 + F_t = W_1 + W_2 - L = 0, \tag{7}$$

where the right-hand side of the equality makes use of the assuption given in Eq. (2). Note that a normal impact condition is considered in this work and a descent velocity $V_0 = 8.86$ ft/s is used at the instant the wheels first touch the ground [33].

B.   A conventional oleo-pneumatic shock absorber

Fig. 2 illustrates the schematic view of a conventional oleo-pneumatic shock absorber. The hydraulic fluid is within the lower chamber of the strut and the pressurized gas is contained in the upper chamber. When the strut is compressed, the fluid is forced through the orifice producing a damping force. Meanwhile, the air is compressed by the piston and provides a gas spring force [34]. The internal friction forces between the bearing and cylinder walls are ignored in this work. Then the total strut force can be expressed by

$$F_s = F_h + F_a, \tag{8}$$

where F_h and F_a denote the hydraulic damping force and air spring force, respectively.

The hydraulic resistance in the shock strut results from the pressure difference associated with flow through the orifice and provides a velocity-squared damping force, governed by

$$F_h = A_d \dot{s}_s |\dot{s}_s|, \tag{9}$$

where the damping factor A_d can be expressed as

$$A_d = \frac{\rho A_h^3}{2C_d A_n^2}.$$ (10)

Here ρ is the mass density of the fluid, A_h is the hydraulic area, C_d is the orifice discharge coefficient and A_n is the net orifice area. According to the polytropic law for the compression of gas, the air spring force is expressed as

$$F_a = p_{a_0} A_a \left(\frac{v_0}{v_0 - A_a s_s}\right)^n,$$ (11)

where p_{a_0} is the initial strut air pressure, A_a is the pneumatic area, v_0 is the initial air volume and n is the effective polytropic exponent for the air-compression process. Further details of the shock absorber model can be found in [33].
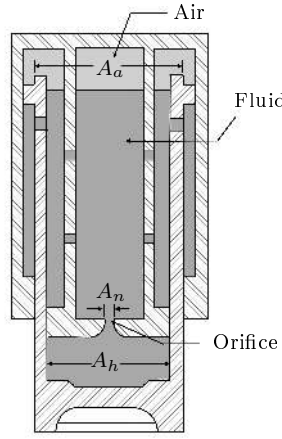

Fig. 2 Schematic view of the oleo-pneumatic shock strut (inspired by [33]).

The parameter values of the landing gear touch-down model and the conventional shock absorber used in [33] and in this paper are summarized in Table 1. A few values (noted by *) were not given in [33] but have been provided in Table 1 by matching the responses shown in [33].

6

Table 1 The parameter values used in the analysis

Parameter	Name	Value	Unit
A_a	Pneumatic area	0.05761	ft^2
$A_d{}^*$	Damping factor of oil damping	339.5	lb$_F \cdot$ s^2/ft^2
g	Gravitational constant	32.18	ft/s^2
$k_t{}^*$	Vertical tire stiffness	18500.0	lb$_F$/ft
n	Polytropic exponent for air-compression process	1.12	-
p_{a_0}	Initial air pressure	6264	lb$_F$/ft^2
v_0	Initial air volume	0.03545	ft^3
V_0	Descent velocity	8.86	ft/s
W_1	Weight of upper mass	2411	lb$_F$
W_2	Weight of lower mass	131	lb$_F$
ϕ^*	Rake angle	12.0	$^\circ$

C.   Proposed performance criteria

Based on the design requirements, namely, to dissipate all the impact energy with the greatest energy absorption efficiency while minimizing gear load, four performance criteria are considered in this work. Firstly, the shock-strut efficiency, η_s, is of significant interest because it indicates the energy absorption ability of the shock strut. Following [5], η_s is defined as

$$\eta_s = \frac{\int_0^{s_{smax}} F_s ds_s}{s_{smax} F_{smax}} \tag{12}$$

where F_{smax} and s_{smax} are the maximum strut load and stroke during the touch-down process, as shown in Fig. 3. The second criterion is the maximum load transmitted by the shock strut to the fuselage, F_{smax}. This is of significance when considering passenger discomfort and the potential for structural damage. Considering the space limit of a landing gear, the maximum strut stroke s_{smax} is used as the third criterion. In addition, the kinetic energy of the aircraft at the end of touch-down process is treated as the last performance criterion. Specifically, the absolute value of the aircraft vertical velocity at the end of touch-down process, $|V_{end}|$, is used to represent such criterion, which

is given by

$$|V_{end}| = |\dot{z}_1(t_{end})| , \tag{13}$$

where t_{end} marks the end of the compression stroke, when $\dot{z}_1 - \dot{z}_2 = 0$ for the first time after the wheels touch the ground. Each of the first three performance criteria will be used as the optimization objective function. Specifically, it is desirable for η_s to be maximized while F_{smax} and s_{smax} should be minimized.
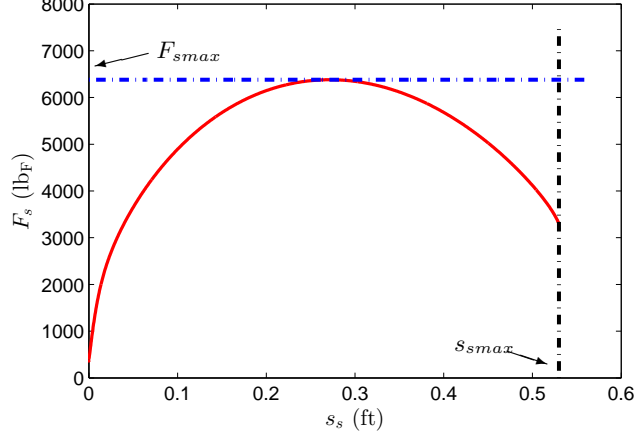

Fig. 3 Load-stroke curve obtained by the conventional oleo-pneumatic shock absorber.

III.   Optimization results and energy analysis

In this section, four candidate shock-strut layouts are proposed. The response of the landing gear with the conventional nonlinear oleo-pneumatic shock absorber is treated as the baseline. Optimizations are carried out using three different objective functions, the strut efficiency, the maximum strut load and the maximum stroke. The beneficial shock-strut configurations and the corresponding performance benefits are identified. In the following discussion, we use the notation 'L' to specify the mechanical network layout and 'C' to specify the configurations which represent optimized layouts with the value for each element identified.

A.   Optimization procedure and candidate layouts

For the default conventional nonlinear shock strut, using the values in Table 1, it can be calculated that $\eta_{sd} = 81.5\%, F_{smaxd} = 6380.3\,\mathrm{lb_F}, s_{smaxd} = 0.53\,\mathrm{ft}$ and $|V_{endd}| = 2.09\,\mathrm{ft/s}$ (the additional

subscript 'd' stands for 'default'). Amongst the four performance criteria introduced in Section II.C, η_s, F_{smax} and s_{smax} will each be used as the optimization objective function with the constraint that the remaining three performance criteria must be no worse than that with the default configuration. For all the optimizations carried out in the present work, we used the Matlab command `patternsearch` first and then `fminsearch` for fine-tuning of the parameters. Note that during the optimization process, no restriction due to practical implementation consideration is placed on the parameter values. Instead we consider whether the parameter values are practical after the optimization stage.

Fig. 4 illustrates the four candidate shock-strut layouts: L1 is the conventional parallel spring-damper layout; L2 is a parallel spring-damper-inerter layout; L3 is the layout of a series inerter-damper arrangement in parallel with a spring; LY represents a general shock-strut layout with a spring in parallel. Layouts L1–L3 are proposed to allow an investigation of the potential performance advantages of layouts with the lowest complexity. Note that for each layout, the spring in parallel, k_s, ensures that the landing gear is capable of supporting the aircraft at the rest position. The lower bound for the stiffness of this spring is set such that the deflection of the gear matches that of the default gear when statically supporting the aircraft ($s_s = 0.50$ ft for a force of $2464.9\,\mathrm{lb_F}$), giving

$$\overline{k}_s = 4884.2\,\mathrm{lb_F/ft}. \tag{14}$$

For each layout, optimizations will be conducted for the case where $k_s = \overline{k}_s$ and for $k_s > \overline{k}_s$.
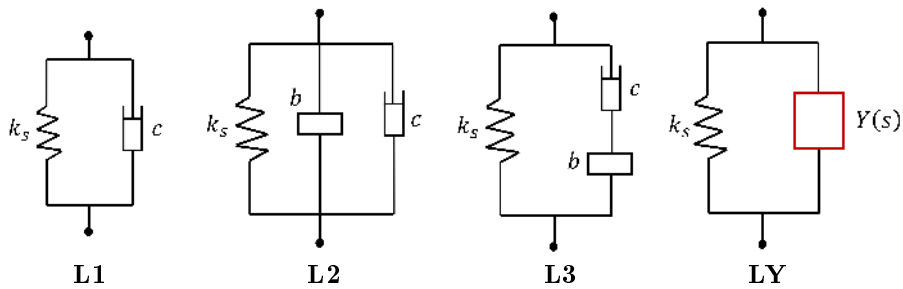

Fig. 4 Four candidate shock-strut layouts.

Layout LY allows for a more complex mechanical structure to be used for improving the touch-down performance. It is represented by a general positive-real frequency function $Y(s)$, which can

be realized by a network consisting of springs, dampers and inerters using the network synthesis method [35]. Similar to layouts L1–L3, the parallel spring k_s is also included in LY to ensure that the gear has sufficient static stiffness. The force-velocity relationship of this layout is given by

$$\widetilde{F_s}(s) = (Y(s) + \frac{k_s}{s})\tilde{s}_s(s), \tag{15}$$

where s is the Laplace variable, $\widetilde{F_s}(s)$ and $\tilde{s}_s(s)$ represent the force and the relative velocity of the strut in the Laplace domain, respectively. In order to obtain relatively low-complexity layouts while covering a reasonable range of possibilities, $Y(s)$ is set to be a biquadratic function, in which the numerator and denominator are second-order functions of the Laplace variable,

$$Y(s) = \frac{As^2 + Bs + C}{Ds^2 + Es + F}. \tag{16}$$

The parameter values $(A, B, \cdots, F)$ are selected through the optimization with the condition that they are all non-negative. For mechanical vibration absorbers, minimizing network complexity is crucial due to space and weight limit. A series of network synthesis results have recently been obtained on efficient realizations of the positive-real biquadratic impedances expressed in Eq. (16) ([36–38]). For the case where k_s is fixed to $\overline{k}_s$, the constraint $F > 0$ is included to ensure that $Y(s)$ does not require an additional parallel spring to supplement k_s. Based on the values of $A, B, \cdots, F$ identified via optimization, the relevant network can be identified and normally contains at least five elements. Then to examine whether a simpler layout may be used, a simplification procedure is employed. Firstly, we study whether the performance deteriorates notably when the least significant element(s) is/are removed. Similar procedures have been successfully demonstrated in [18, 25]. Secondly, a new optimization is carried out for the remaining element values based on this simplified network layout.

B. Identified beneficial configurations

The optimization results are summarized in Tables 2 and 3. Note that the subscripts η, F and s are used to indicate the results using η_s, F_{smax} and s_{smax} as the objective function, respectively; v is used to specify the case when k_s is allowed to be variable (the $k_s > \overline{k}_s$ case).

<div align="center">

Table 2 Optimization results using layouts L1–L3†

</div>

Configurations	Performance			Layouts	Optimum parameter values
	η_s	$F_{smax}(\mathrm{lb_F})$	$s_{smax}(\mathrm{ft})$		$(\mathrm{lb_F/ft},\ \mathrm{lb_F \cdot s/ft},\ \mathrm{lb_m})$
Default	81.5%	6380.3	0.53	-	-
C1$_{\eta v}$	84.7%(3.9%)	5787.4	0.53	L1	$k_s = 7126.2, c = 796.1$
C2$_{\eta v}$	90.0%(10.4%)	5353.4	0.53	L2	$k_s = 9159.8, c = 519.5, b = 9.4$
C3$_{\eta v}$	92.8%(13.9%)	5248.5	0.50	L3	$k_s = 19492, c = 40715, b = 9.4$
C1$_{Fv}$	81.9%	5581.0(12.5%)	0.53	L1	$k_s = 9043.9, c = 535.2$
C2$_{Fv}$	92.4%	5014.5(21.4%)	0.53	L2	$k_s = 16163, c = 60.21, b = 18.1$
C3$_{Fv}$	92.3%	5003.9(21.6%)	0.53	L3	$k_s = 16927, c = 12171, b = 19.2$
C1$_{sv}$	81.5%	6380.3	0.43(18.9%)	L1	$k_s = 12109.6, c = 772.6$
C2$_{sv}$	88.5%	6380.3	0.37(30.2%)	L2	$k_s = 22794, c = 374.3, b = 19.4$
C3$_{sv}$	83.2%	6380.3	0.39(26.4%)	L3	$k_s = 22755, c = 1471.8, b = 33.3$

† % improvements are given in bracket for the criteria being optimized. Same notations apply to other tables in this work.

Considering layouts L1–L3, no improvement over the default system was identified for the case where $k_s = \overline{k}_s$. Hence Table 2 only summarized the results for the $k_s > \overline{k}_s$ case. The configuration C1$_{\eta v}$ can provide a 3.9% improvement in η_s, which is not significant compared with configurations C2$_{\eta v}$ and C3$_{\eta v}$, where up to 10.4% and 13.9% performance improvements can be obtained, respectively. The benefits of including an inerter can be seen by comparing the performance obtained with C2$_{\eta v}$ and C3$_{\eta v}$ to that of the inerter-free C1$_{\eta v}$. Improvements in η_s performance of 6.3% and 9.6%, respectively, are achieved, which can be attributed to the inclusion of an inerter. However, it should be noted that in C3$_{\eta v}$ a much higher damping value is required, which is likely to be impractical. Further optimizations found that the performance benefits seen with C3$_{\eta v}$ will be reduced if we adopt a smaller damper. In order to achieve the same level of improvement in η_s as C2$_{\eta v}$, i.e. 10.4%, the damping required for the optimal C3$_{\eta v}$ is nearly triple that of C2$_{\eta v}$ and the inertance is doubled. Therefore, we take the view that C2$_{\eta v}$ is more beneficial than C3$_{\eta v}$ from the practicality perspective. Results with F_{smax} as the objective function indicate that C1$_{Fv}$ can reduce F_{smax} by

12.5% compared with the default performance, and 21.4% and 20.7% improvements can be obtained respectively by the optimum configurations $C2_{Fv}$ and $C3_{Fv}$. Similar to the efficiency optimization case, it can be seen that a large damping is required for $C3_{Fv}$ and a reduced damping leads to a reduced performance improvement. For the optimization over s_{smax}, it can be seen that $C1_{sv}$ helps reduce s_{smax} by 18.9% compared with the default configuration. In addition, for $C2_{sv}$ and $C3_{sv}$, the percentage improvements compared with the default performance are 30.2% and 26.4%, respectively.

The optimum results for layout LY are summarized in Table 3. In contrast to the simpler layouts L1–L3, when fixing k_s, a 14.0% improvement in strut efficiency can be obtained by CY_η. Using relevant network synthesis theory, its mechanical network is realized by a configuration consisting of three dampers, one inerter, one spring and k_s. However, two of the dampers can be removed since their values are small (when in parallel) or large (when in series) compared with the remaining ones. Thus the mechanical layout of CY_η, labelled L4, is a four-element network, as shown in Fig. 5. A further optimization over L4 in which b is removed is carried out but no optimal solution is found. This suggests that the performance improvement obtained by CY_η using L4 requires the inclusion of the inerter. Configuration $CY_{\eta v}$ provides the maximum improvement in η_s, however a much more complex network, nine-element network excluding k_s, is required. The slight performance improvement compared with CY_η probably does not compensate for the difficulty in design and manufacture of this configuration, hence we disregard it. It can be seen from Table 3 that a 21.6% improvement in F_{smax} can be obtained by the configuration CY_F. The network realization of this transfer function is identified and shown in Fig. 5 as layout L5. In this layout, an inerter is in parallel with the supporting stiffness, as well as a combination of two dampers and an internal spring. Note that layout L5 can be reduced to L2 if c_1 in L5 is set to infinity. The similarities of the parameter values between the two configurations, CY_F and $C2_{\eta v}$, are observed. The maximum performance advantage using F_{smax} as the objective function is obtained by CY_{Fv}, with up to 22.0% improvement. The resulting mechanical network, labelled L6, is illustrated in Fig. 5. Note that layouts L5 and L6 consist of five mechanical elements but in different arrangements. As for optimizing over s_{smax}, the case with a fixed supporting stiffness, $k_s = \overline{k}_s$, a maximum improvement

12

of only 5.7% is obtained. Allowing k_s to vary results in more complex layouts than L2 and L3 but with no improvements over them. Hence the s_{smax} objective function results are not listed in Table 3.

Table 3 Optimization results using layout LY

Configurations	Performance			Layouts	Optimum parameter values
	η_s	$F_{smax}(\mathrm{lb_F})$	$s_{smax}(\mathrm{ft})$		$(\mathrm{lb_F/ft},\ \mathrm{lb_F \cdot s/ft},\ \mathrm{lb_m})$
Default	81.5%	6380.3	0.53	-	-
CY_η	92.9%(14.0%)	5187.0	0.50	L4	$k_s = 4884.2, c = 5362.9, k_1 = 15633,$ $b = 19.7$
$\mathrm{CY}_{\eta v}$	93.2%(14.4%)	5266.3	0.49	-	-
CY_F	91.2%	5004.9(21.6%)	0.53	L5	$k_s = 4884.2, c_1 = 3817.1, c_2 = 404.9,$ $b = 9.4, k_1 = 6874.1$
CY_{Fv}	92.0%	4976.5(22.0%)	0.53	L6	$k_s = 8049.2, c_1 = 8492.6, c_2 = 9089.1,$ $b = 20.6, k_1 = 9031.3$
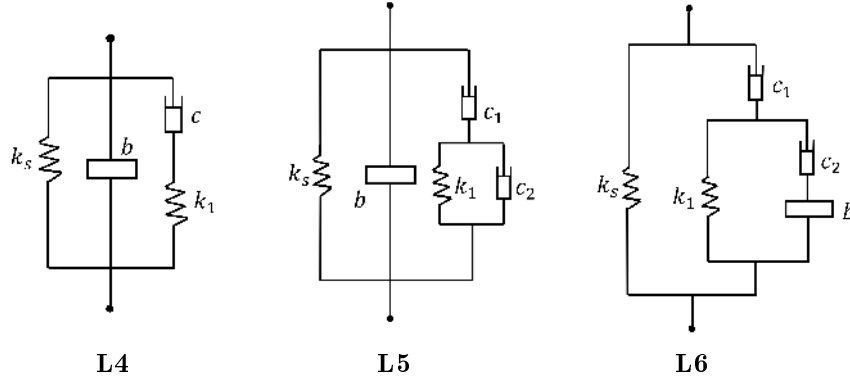
Fig. 5 Layouts L4–L6, which corresponds to configurations CY_η, CY_F and CY_{Fv}.

In summary, considering the performance improvements and practical parameter values, we treat $\mathrm{C2}_{\eta v}$ and CY_η as the optimum configurations for the η_s performance, $\mathrm{C2}_{Fv}$, CY_F and CY_{Fv} as the optimum configurations for F_{smax} performance, and $\mathrm{C2}_{sv}$ and $\mathrm{C3}_{sv}$ as the optimum configurations for s_{smax} performance. Also of interest are $\mathrm{C1}_{\eta v}$, $\mathrm{C1}_{Fv}$ and $\mathrm{C1}_{sv}$, as linear configurations in which no inerter is present. The load-stroke curves provided by these configurations, as well as the default

one, are compared in Fig. 6. Note that the curves in Fig. 6 all finish at the end of the compression stroke. The shorter curves in Fig. 6(a) and (c) indicate that when the first compression process is finished, the maximum strokes the struts reach are smaller than the baseline system.
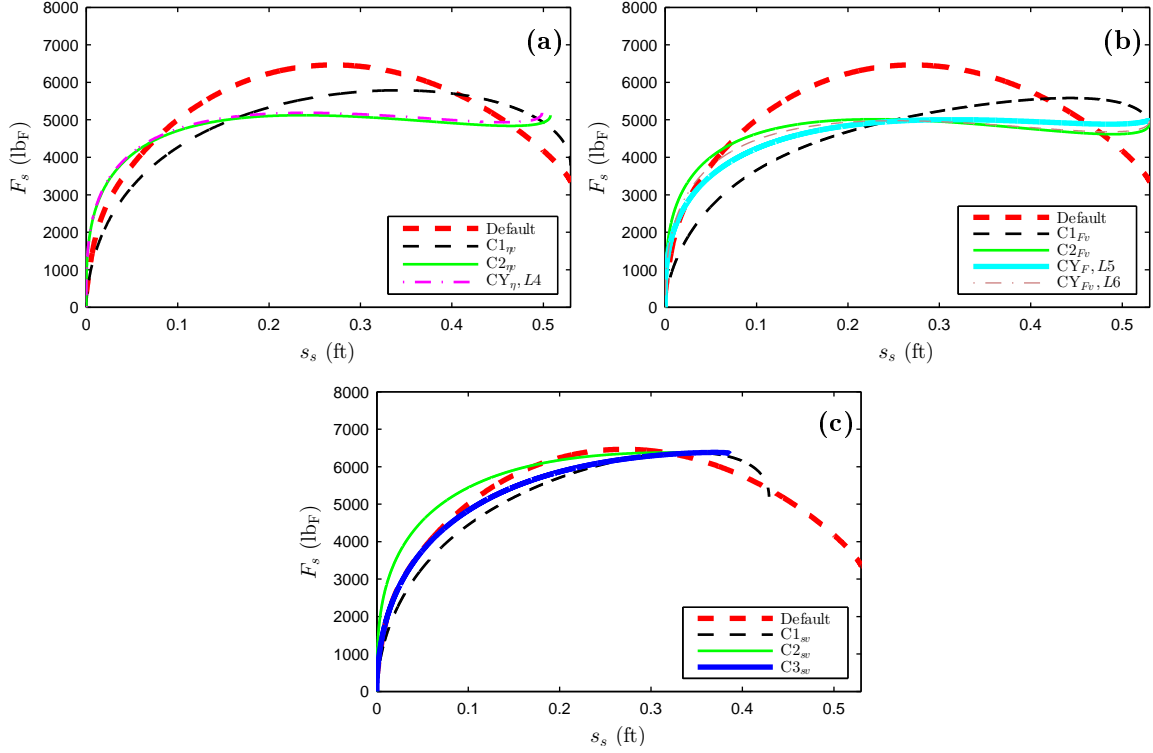

Fig. 6 The load-stroke curves improving (a) η_s, (b) F_{smax} and (c) s_{smax}.

C. Energy analysis of beneficial inerter-based struts

Up to this point, we have considered the energy absorption ability of the strut using η_s. A more detailed investigation into how much energy is dissipated and stored during touch-down process is now presented. The work-energy principle can be applied, to give

$$\Delta E_k + \Delta E_p = W_d + W_L, \tag{17}$$

where ΔE_k and ΔE_p represent the change of the kinetic and potential energy in the system, W_d and W_L are the work done by the damper(s) of the strut and the lifting force L, respectively. Here,

$$\Delta E_k = E_k(t_{end}) - E_k(0), \tag{18}$$

$$\Delta E_p = -W_1 \cdot z_1(t_{end}) - W_2 \cdot z_2(t_{end}) + E_{pt} + E_{ps}, \tag{19}$$

14

$$W_L = -L \cdot z_1(t_{end}), \tag{20}$$

where $E_k(0)$ and $E_k(t_{end})$ denote the kinetic energy of the system just prior to the tires making contact with the ground and at the end of the compression stroke respectively. E_{pt} and E_{ps} are the potential energy stored in the tires and the shock struts at the end of the process, respectively. Substituting Eqs. (1), (2), (18), (19), and (20) into (17) gives

$$E_k(0) = E_k(t_{end}) + E_{pt} + E_{ps} - W_d + W_2 \cdot s_s \cdot cos\phi, \tag{21}$$

which means the original kinetic energy of the system is transformed partially to the stored potential energy in the tires and the strut, the work done by the gravity, as well as dissipated by the strut.

Table 4 Energy distributions of the beneficial configurations

Configurations	$E_k(t_{end})(\text{lb}_\text{F} \cdot \text{ft})$	$E_{pt}(\text{lb}_\text{F} \cdot \text{ft})$	$E_{ps}(\text{lb}_\text{F} \cdot \text{ft})$	$(-W_d)(\text{lb}_\text{F} \cdot \text{ft})$	$W_2 \cdot s_s \cdot cos\phi(\text{lb}_\text{F} \cdot \text{ft})$
Default	172.5	230.1	353.7	2157.5	67.8
C1$_{\eta v}$	151.8	400.8	955.4	1525.7	67.8
C2$_{\eta v}$	18.3	576.5	1170.3	1268.2	67.8
CY$_\eta$(L4)	146.7	595.2	1941.6	353.4	67.8
C1$_{Fv}$	73.9	645.9	1212.5	1100.9	67.8
C2$_{Fv}$	172.5	517.5	2156.4	186.7	67.8
CY$_F$(L5)	0.2	722.8	1225.0	1085.1	67.8
CY$_{Fv}$(L6)	156.0	561.3	2153.5	162.3	67.8
C1$_{sv}$	156.4	760.2	1064.3	1065.1	54.9
C2$_{sv}$	7.0	1076.7	1463.8	540.0	46.8
C3$_{sv}$	0.2	1094.1	1665.2	292.2	49.4

Table 4 summarizes the individual energy distributions by the default nonlinear and optimal shock-strut configurations. Note $E_k(0)$ is not included in the Table since this term is the same for all configurations, $E_k(0) = 3100.5 \, \text{lb}_\text{F} \cdot \text{ft}$. It can be seen that the term $W_2 \cdot s_s \cdot cos\phi$ is small compared with E_{pt}, E_{ps} and $-W_d$. Therefore, Table 4 illustrates that the reduced kinetic energy is mostly transformed to the potential energy, stored in the tires and shock struts, as well as the energy dissipated by the damping effects of the shock strut. It can also be seen that the maximum work

done by the dampers $-W_d$ is achieved by C2$_{\eta v}$, which is still significantly less than that achieved by the the default strut. Moreover, compared with the default configuration, more potential energy is stored in the shock strut, as well as in the tire compliance. This will pose challenges for the design of the strut elongation process and may even lead to a rebound. Hence an energy dissipation constraint is implemented in the next section.

IV. Optimization results with an energy dissipation constraint

Further investigations with an extra constraint on energy dissipation are discussed in this section. It will be shown that with this constraint, limited improvements can be provided by the layouts proposed in Section III. The reason for reduced improvements will be discussed. Configurations with a double-stage supporting spring are then proposed, which can achieve significant performance advantages.

A. Identified beneficial configurations with a linear supporting spring

To ensure good energy dissipation capability, the constraint that the energy dissipation is no less than that by the conventional strut, 2157.5 lb$_F$, is implemented. However, the optimizations found no results if considering 2157.5 lb$_F$ as the energy dissipation constraint directly. This is because a linear spring with $k_s \geq 4884.2$ lb$_F$/ft is used as the static spring here. Such a spring stores more potential energy at the end of touch-down process than that of the nonlinear spring in the default system. Then with the energy dissipation constrained to be no less than 2157.5 lbF, the total work done by the linear strut is inevitably more than the nonlinear system, resulting in either F_{smax} or s_{smax} exceeding their constraints. Two approaches are considered here to overcome this, firstly the energy dissipation constraint requirement is relaxed by 10% to 1941.8 lb$_F$. Later, in Section IV.B, a double-stage static spring is considered. The strut efficiency and the maximum strut load will be used as the objection functions. In addition, k_s is fixed to $\overline{k}_s$ to minimize the potential energy stored in the supporting spring at the end. Note that the maximum stroke will not be optimized since as discussed in Section III.B the static stiffness is fixed and the maximum improvement is limited to 5.7% (from s_{smax} equals 0.53 ft to 0.50 ft).

Table 5 Optimization results with the linear k_s considering the energy dissipation constraint

Configurations	Performance		Layouts	Optimum parameter values	$(-W_d)$
	η_s	$F_{smax}(\text{lb}_\text{F})$		$(\text{lb}_\text{F}/\text{ft},\ \text{lb}_\text{F}\cdot\text{s/ft},\ \text{lb}_\text{m})$	$(\text{lb}_\text{F}\cdot\text{ft})$
Default	81.5%	6380.3	-	-	2157.5
$C4_\eta$	89.3%(9.6%)	6070.13	L4	$k_s = 4884.2, c = 1286.1, k_1 = 43351,$ $b = 24.7$	1941.8
$C5_\eta$	89.3%(9.6%)	6111.8	L5	$k_s = 4884.2, c_1 = 1317.6, c_2 = 2.4 \times 10^{-11},$ $b = 25.1, k_1 = 43927$	1941.8
$C4_F$	88.7%	5803.5(9.0%)	L4	$k_s = 4884.2, c = 1043.2, k_1 = 42033,$ $b = 21.8$	1941.8
$C5_F$	88.7%	5803.7(9.0%)	L5	$k_s = 4884.2, c_1 = 1042.4, c_2 = 0.04,$ $b = 21.9, k_1 = 41706$	1941.8

For the optimization, L4–L6 in Fig. 5, which can provide performance advantages in η_s and F_{smax}, are used as the candidate layouts (subscripts 'η' and 'F' are used to specify). Since the layout L6 exhibited no improvements in the two objective functions, the optimization results are not presented here. Considering layouts L4 and L5, the corresponding configurations are labelled C4 and C5. Table 5 summarizes the performance benefits and parameter values for these configurations. It can be seen that η_s is increased by 9.6% using either $C4_\eta$ or $C5_\eta$ over the default configuration. The optimization gives $c_2 = 2.4 \times 10^{-11}$ $\text{lb}_\text{F} \cdot \text{s/ft}$ for $C5_\eta$, suggesting that removing c_2 is possible to simplify this configuration. Hence $C4_\eta$ (row 2) is the most optimum configuration for this case, and its load-stroke curve is plotted in Fig. 7(a). Considering F_{smax}, it is found that the maximum benefit over the default configuration is obtained by $C4_F$, with a 9.0% improvement. Again we find that the $C5_F$ configuration simplifies to C4 (as c_2 is small, see row 5 of Table 5). The load-stroke curves with the conventional strut and $C4_F$ (row 4) are plotted in Fig. 7(b). Note that in this optimization case, L1–L3, and L4 with the inerter excluded, do not provide any improvement in η_s or F_{smax} comparing with the baseline system. This suggests that the performance benefits using layout L4 are attributed to the inclusion of the inerter. For both objective functions, the improvements listed in Table 5 compared to Table 3 are reduced. This is because if we consider

17

the energy dissipation constraint, namely, $(-W_d) \geq 1941.8\,\mathrm{lb_F} \cdot \mathrm{s/ft}$, the total work done by the optimized shock strut here exceeds that of the cases without the energy dissipation constraint. This may lead to a higher F_{smax} and also a worse η_s performance. Rather than considering a minimum energy dissipation constraint of $1941.8\,\mathrm{lb_F}$ (10% less than the default) if we consider $2157.5\,\mathrm{lb_F}$ (5% less), the performance improvement of η_s with the layout L4 is reduced to 5.6%, but with the advantage that the extension stroke is likely to be improved.
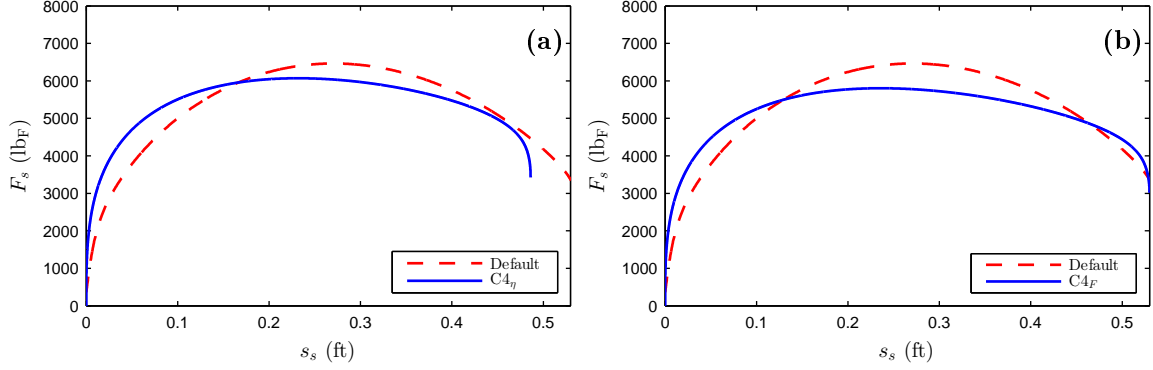

Fig. 7 The load-stroke curves obtained with (a) C4$_\eta$ and (b) C4$_F$.

B. Proposing double-stage supporting spring

Recall that the minimum spring stiffness $k_s = \overline{k}_s$ was selected such that the spring deflection matched that of the air spring when subjected to the aircraft static load. This point is indicated by a red dot in Fig. 8. The figure shows the force-deflection relationship for the full compression stroke (up until $s_{smax} = 0.53$ ft). It can be seen that during the compression of the spring the stored energy of the linear spring far exceeds that of the nonlinear device. When the energy dissipation constraint is considered, the limitation of performance benefits is inevitable as discussed in Section IV.A.

A supporting spring with a double-stage, or progressive-rate, supporting stiffness is now introduced. The force-stroke relationship of the double-stage spring is given as

$$
F_k = \begin{cases} k_{s1} s_s & \text{if } s_s \leq s_{sx} \\[2mm] k_{s2}(s_s - s_{sx}) + F_{sx} & \text{if } s_s > s_{sx} \end{cases}
$$

where F_k is the supporting spring force, k_{s1} and k_{s2} are the two spring rates. Here s_{sx} and F_{sx} are

the stroke and spring force where the two rates intersect in the force-stroke curve and are treated as parameters to be optimized. As with the linear spring k_s, the double-stage one is designed to support the aircraft under the same stoke with the nonlinear air spring. An example force-displacement relationship is shown in Fig. 8. From the figure it can been seen that the double-stage supporting spring provides the possibility that its stored potential energy (right-slanted-shading region in Fig. 8) could be less than that by the nonlinear spring (left-slanted-shading region in Fig. 8) when reaching the maximum stroke.
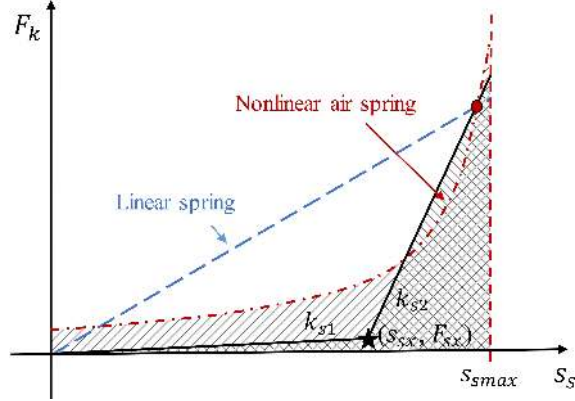

Fig. 8 Force-deflection relationships with the air spring and two kinds of k_s.

C. Identified beneficial configurations with a double-stage supporting spring

If we use the double-stage spring in the L1 layout, the optimization can identify considerable improvements in performance, which are 7.6% in η_s by C1$_{\eta2}$ and 14.1% in F_{smax} by C1$_{F2}$. However, we can not regard these configurations as beneficial ones since the load-stroke curve provided by C1$_{\eta2}$ or C1$_{F2}$ experiences a sudden change. We take C1$_{\eta2}$ as an example here. The parameter values of C1$_{\eta2}$ are summarized in Table 6 and the load-stroke curves obtained with the default and C1$_{\eta2}$ (black line) configurations are illustrated in Fig. 9(a). It can be seen that the upper and lower masses will also undergo sudden changes in their accelerations towards the end of the stroke, which will lead to passenger/crew discomfort and additional structural loading. Similar conclusions can be obtained for C1$_{F2}$, as well as the optimization using L2 and L3. Therefore, we will not include the results of the optimal C1−C3 with a double-stage spring here. Instead, since the layout L4 is regarded as the most optimum layout in the previous optimization, this layout will be used as an

example layout to illustrate the benefits of the double-stage supporting spring. Note that the exact energy dissipation constraint, $(-W_d) \geq 2157.5\,\text{lb}_\text{F} \cdot \text{s/ft}$, is considered in this case. The results of optimization are illustrated in Table 6. The subscript '2' is used to specify this case. It can be seen that up to 11.9% improvement in η_s can be obtained using the configuration $C4_{\eta 2}$. Moreover, the layout with different parameter values, i.e. $C4_{F2}$ can also reduce F_{smax} by 20.0% comparing with the default configuration which represents a significant improvement of the 9.0% reduction achieved with the linear spring ($C4_F$, Table 5). The load-stroke curves for these two configurations are illustrated in Fig. 9. We note that for both cases the first stage stiffness is negligible.

Table 6 Optimization results with the double-stage k_s considering the energy dissipation constraint

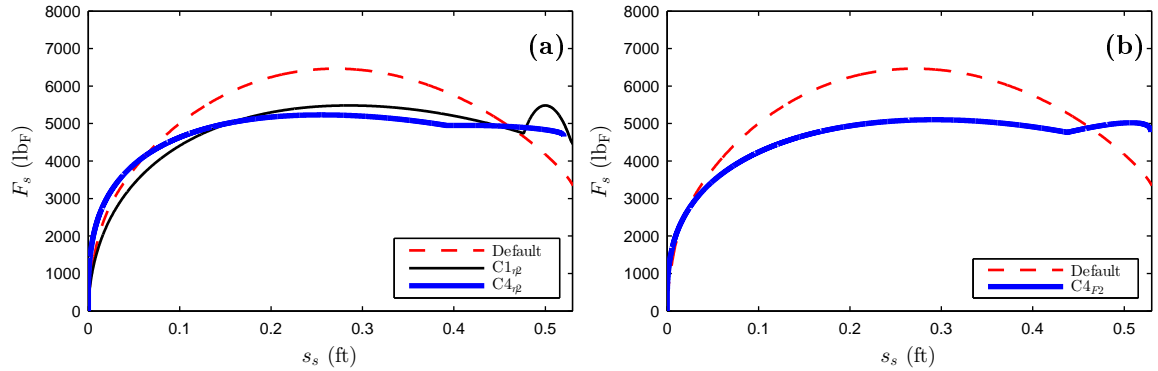| Configurations	Performance		Layouts	Optimum parameter values	$(-W_d)$
	η_s	$F_{smax}(\text{lb}_\text{F})$		$(\text{lb}_\text{F}/\text{ft}, \text{lb}_\text{F} \cdot \text{s/ft}, \text{lb}_\text{m})$	$(\text{lb}_\text{F} \cdot \text{ft})$
Default	81.5%	6380.3	-	-	2157.5
$C1_{\eta 2}$	87.7%(7.6%)	5482.0	L1	$k_{s1} = 520.1, k_{s2} = 78344, c = 975.9$	2157.5
$C4_{\eta 2}$	91.2%(11.9%)	5230.7	L4	$k_{s1} = 0.9, k_{s2} = 22011, c = 1060.7,$	2157.5
				$b = 15.4, k_1 = 43697$	
$C4_{F2}$	90.10%	5101.5(20.0%)	L4	$k_{s1} = 3.1, k_{s2} = 36899, c = 985.1,$	2157.5
				$b = 10.4, k_1 = 53305$	

Fig. 9 The load-stroke curves obtained with (a) $C1_{\eta 2}$, $C4_{\eta 2}$, and (b) $C4_{F2}$.

V.   Conclusions

This paper has investigated the potential aircraft touch-down performance benefits with inerter-integrated shock struts for a landing gear. Based on a 2DoF model with the conventional oleo-pneumatic shock absorber, the baseline touch-down performances are obtained. Guaranteeing that the optimum shock struts absorb at least the same level of kinetic energy as the baseline system, the optimizations have been carried out. Using three different objective functions, the strut efficiency, the maximum strut load and the maximum strut stroke, up to 14.0%, 22.0% and 30.2% improvements are obtained respectively. The advantages of the inclusion of an inerter have also been investigated. An energy analysis shows that for the beneficial configurations, more potential energy will be stored in the strut and via tire compliance at the end of the strut compression process. Hence an energy dissipation constraint is implemented and the beneficial layouts obtained in the previous optimization are used as the candidate layouts. The objective functions of the strut efficiency and the maximum strut load are considered and the performance improvements are reduced to 9.6% in the strut efficiency and 9.0% in the maximum strut load. It has then be presented that the limitation on performance benefits lies in the energy dissipation constraint and the linear supporting stiffness used. Then configurations with double-stage supporting springs are introduced. It has been shown that up to 11.9% and 20.0% improvements in the strut efficiency and the maximum strut load can be obtained, respectively.

References

[1] Wang, X., and Carl, U., "Fuzzy Control of Aircraft Semi-active Landing Gear System," *Proceeding of the 37th AIAA Aerospace Sciences Meeting and Exhibit*, Reno, NV, AIAA Paper 1999-265, 1999.

[2] Niu C., "Airframe Structural Design: Practical Design Information and Data on Aircraft Structures," Conmilit Press, Hong Kong, 1988.

[3] Jenkins, S. F. N., "Landing Gear Design and Development," *Proceedings of the Institution of Mechanical Engineers, Part G: Journal of Aerospace Engineering*, Vol. 203, No. 1, 1989, pp. 67–73.

[4] Hitch, H. P. Y., "Aircraft Ground Dynamics," *Vehicle System Dynamics*, Vol. 10, No. 4-5, 1981, pp. 319–332.

[5] Currey, N. S.,"Aircraft Landing Gear Design: Principles and Practices," AIAA Education, New York, 1988.

[6] Howell, W., McGehee, J. R., Daugherty, R. H., and Vogler, W. A., "F-106B Airplane Active Control Landing Gear Drop Test Performance," NASA TM 102741, 1990.

[7] Horta, L. G., Daugherty, R. H., and Martinson, V. J., "Modeling and Validation of a Navy A6-Intruder Activity Controlled Landing Gear System," NASA TP 209124, 1999.

[8] Choi, Y.T., and Wereley, N.M., "Vibration Control of A Landing Gear System Featuring Electrorheological/Magnetorheological Fluids," *Journal of Aircraft*, Vol. 40, No. 3, 2003, pp. 432–439. doi:10.2514/2.3138

[9] Krüger, W., "Design and Simulation of Semi-active Landing Gears for Transport Aircraft." *Mechanics of Structures and Machines*, Vol. 30, No. 4, 2002, pp. 493–526.

[10] Smith, M. C., "Synthesis of Mechanical Networks: the Inerter," *IEEE Transactions on Automatic Control*, Vol. 47, No. 10, 2002, pp. 1648–1662.

[11] Jiang, J.Z., Matamoros-Sanchez, A.Z., Goodall, R.M., and Smith, M.C., "Passive Suspensions Incorporating Inerters for Railway Vehicles," *Vehicle System Dynamics*, Vol. 50, No. sup1, 2012, pp. 263–276.

[12] Jiang, Z., Matamoros-Sanchez, A.Z., Zolotas, A., Goodall, R., and Smith, M.C., "Passive Suspensions for Ride Quality Improvement of Two-axle Railway Vehicles," *Proceedings of the Institution of Mechanical Engineers, Part F: Journal of Rail and Rapid Transit*, 2013.

[13] Scheibe, F., and Smith, M.C., "Analytical Solutions for Optimal Ride Comfort and Tyre Grip for Passive Vehicle Suspensions," *Vehicle System Dynamics*, Vol. 47, No. 10, 2009, pp. 1229–1252.

[14] Jiang, J. Z., Smith, M. C., and Houghton, N. E., "Experimental Testing and Modelling of a Mechanical Steering Compensator", *The 3rd Int. Symp. Communications, Control Signal Processing (ISCCSP)*, 2007, pp. 249–254.

[15] Limebeer, D., Sharp, R., Evangelou, S., and Smith, M., "An H$_\infty$ Loop-Shaping Approach to Steering Control for High-Performance Motorcycles," *Lecture notes in Control and Information Sciences*, Vol. 329, Springer, New York, 2006, pp. 257–275.

[16] Wang, F. C., Chen, C. W., Liao, M. K., and Hong, M. F., "Performance Analyses of Building Suspension Control with Inerters," *Decision and Control*, IEEE, 2007, pp. 3786–3791.

[17] Lazar, I. F., Neild, S. A., and Wagg, D. J., "Using an Inerter-based Device for Structural Vibration Suppression," *Earthquake Engineering & Structural Dynamics*, Vol. 43, No. 8, Wiley Online Library, 2014, pp. 1129–1147.

[18] Zhang, S.Y., Jiang, J.Z., and Neild, S. A., "Optimal Configurations for A Linear Vibration Suppression Device in A Multi-storey Building," *Structural Control and Health Monitoring*, 2016. doi: 10.1002/stc.1887

[19] Jiang, J.Z., Matamoros-Sanchez, A.Z., Goodall, R.M. and Smith, M.C., "Passive Suspensions Incorporating Inerters for Railway Vehicles," *Vehicle System Dynamics*, Vol. 50, No. sup1, 2012, pp. 263–276.

[20] Wang, F.C., Liao, M.K., Liao, B.H., Su, W.J., and Chan, H.A., "The Performance Improvements of Train Suspension Systems with Mechanical Networks Employing Inerters," *Vehicle System Dynamics*, Vol. 47, No. 7, 2009, pp. 805–830.

[21] Jiang, Z., Matamoros-Sanchez, A.Z., Zolotas, A., Goodall, R., and Smith, M., "Passive Suspensions for Ride Quality Improvement of Two-axle Railway Vehicles," *Proceedings of the Institution of Mechanical Engineers, Part F: Journal of Rail and Rapid Transit*, 2013.

[22] Mcbeath, S., "Shocks to the System," Racecar Engineering, Nov. 2011.

[23] Xin, D., Yuance, L., and Chen, M.Z., "Application of Inerter to Aircraft Landing Gear Suspension," *34th Chinese Control Conference*, IEEE, 2015, pp. 2066–2071.

[24] Liu, Y., Chen, M.Z., and Tian, Y., "Nonlinearities in Landing Gear Model Incorporating Inerter," *IEEE International Conference on Information and Automation*, 2015, pp. 696–701.

[25] Li, Y., Jiang, Z., and Neild, S. A., "Inerter-based Configurations for Main Landing Gear Shimmy Suppression," *Journal of Aircraft*. Online version is available. doi:10.2514/1.c033964

[26] Hu, Y., Chen, M.Z., Shu, Z. and Huang, L., "Vibration Analysis for Isolation System with Inerter," *The 33rd Chinese Control Conference (CCC)*, IEEE, 2014, pp. 6687–6692.

[27] Wang, F.C. and Su, W.J., "Inerter Nonlinearities and The Impact on Suspension Control," *American Control Conference*, IEEE, 2008, pp. 3245–3250.

[28] Gonzalez-Buelga, A., Lazar, I.F., Jiang, J.Z., Neild, S.A. and Inman, D.J., "Assessing the Effect of Nonlinearities on The Performance of A Tuned Inerter Damper," *Structural Control and Health Monitoring*, 2016. doi: 10.1002/stc.1879

[29] Flügge, W., and Coale, C. W., "The Influence of Wheel Spin-up on Landing Gear Impact," NACA TN 3217, 1955.

[30] Cook, F. E., and Milwitsky, B., "Effect of Interaction on Landing Gear Behavior and Dynamic Loads in A Flexible Airplane Structure," NACA Report 1278, 1956.

[31] Walls, J. H., "An Experimental Study of Orifice Coefficients, Internal Strut Pressures, and Loads on a Small Oleo-pneumatic Shock Strut," NACA TN 3426, 1955.

[32] Walls, J. H., "Investigation of the Air-compression Process During Drop Tests of An Oleo-pneumatic Landing Gear," NACA TN 2477, 1951.

[33] Milwitzky, B., and Cook, F. E., "Analysis of Landing Gear Behavior," NACA Report 1154, 1953.

[34] Yadav, D., and Ramamoorthy, R.P., "Nonlinear Landing Gear Behavior at Touchdown," *ASME Journal of Dynamic Systems, Measurement, and Control*, Vol. 113, No. 4, 1991, pp. 677–683.

[35] Bott, R., and Duffin, R.J., "Impedance Synthesis Without Use of Transformers," *Journal of Applied Physics*, Vol. 20, No. 8, 1949, pp. 816–816.

[36] Jiang, J.Z., and Smith, M.C., "Regular Positive-real Functions and Five-element Network Synthesis for Electrical and Mechanical Networks," *IEEE Transactions on Automatic Control*, Vol. 56, No. 6, IEEE, 2011, pp. 1275–1290.

[37] Jiang, J.Z., and Smith, M.C., "Series-parallel Six-element Synthesis of Biquadratic Impedances," *IEEE Transactions on Circuits and Systems I: Regular Papers*, Vol. 59, No. 11, IEEE, 2012, pp. 2543–2554.

[38] Jiang, J.Z., and Smith, M.C., "On the Theorem of Reichert," *Systems & Control Letters*, Vol. 61, No. 12, 2012, pp. 1124–1131.